Reversible Crystallization and Melting at the Lateral Surface of Isotactic Polypropylene Crystals

René Androsch*,† and Bernhard Wunderlich‡

Martin-Luther-University Halle-Wittenberg, Institute of Material Science, Geusaer Str., D06217 Merseburg, Germany, and Department of Chemistry, The University of Tennessee, Knoxville, Tennessee 37996-1600, and Oak Ridge National Laboratory, Chemical and Analytical Sciences Division, Oak Ridge, Tennessee 37831-6197

Received February 12, 2001; Revised Manuscript Received June 8, 2001

ABSTRACT: Reversible crystallization and melting in isotactic polypropylene are suggested to occur at the lateral crystal surface by correlation of the amount of reversibility to the structure observed by atomic force microscopy. The degree of reversibility is monitored on heating using temperature-modulated differential scanning calorimetry. It changes with the crystallization conditions on cooling from the melt. In quenched samples the reversing fraction of the heat flow rate is considerably higher than in well-crystallized specimens. On heating, reversible latent heat develops, starting at about 300 K, just above the glass transition, and continues up to the final melting peak. Irreversible processes in the same temperature range have been separated from the reversible effects and involve cold crystallization, annealing, and a phase transition from the quenched mesophase to the stable crystal form. Because of a similar enthalpy-based crystallinity and crystal thickness in the final melting range above ≈400 K, the difference in reversibility of crystallization and melting can be explained by the observed differences in crystal morphology. The slowly cooled sample consists of well-organized, laterally extended lamellae, while the quenched sample has a distinctly globular crystal morphology which permits an increased lateral surface area. Differential scanning calorimetry yields the temperature dependence of the crystallinity, and temperature-resolved X-ray scattering is employed to monitor changes of the crystals during heating.

1. Introduction

Isotactic polyproyplene (iPP) exhibits different crystal structures and crystal morphologies as a function of crystallization conditions. Cooling from the melt at low or moderate cooling rates leads usually to the formation of the thermodynamically stable monoclinic α-polymorph[1] with a 2*3/1 helical conformation of the molecule. The pseudohexagonal β-structure [2−4] can be observed after crystallization at higher cooling rates or by heterogeneous nucleation using specific β-nucleators, and an orthorhombic γ-structure[3,5,6] develops preferentially in low molecular mass fractions or during crystallization at elevated pressure. At extremely high cooling rates, i.e., by quenching to ambient or subambient temperatures, a mesomorphic, conformationally disordered structure can be observed which is easily recognized by the absence of sharp crystalline reflections; i.e., one detects no obvious long-range order in the wide-angle X-ray diffraction pattern. The enthalpy of the quenched samples reaches a similar level as found in semicrystalline α-polypropylene, somewhere intermediate between the high enthalpy of the melt and the (calculated) low value for 100% crystallinity. This proves that there must be a considerable degree of order between neighboring chains. Infrared spectroscopic studies verify short-range order in quenched iPP with an almost identical conformation as in the α-polymorph.[7] The structure of the mesomorphic phase in quenched specimens was identified by the term "smectic", to point to an array of chains with a better order in longitudinal than in transverse chain direction.[8] Later research revealed that the structure of the mesomorphic phase is close to the structure of the monoclinic α-form, although an unequivocal consent was not achieved.[9−12] The crystallization of the α-form from the melt occurs via chain folding and the formation of a lamellar superstructure. Depending on the crystallization temperature, crosshatching of iPP lamellae is observed as a unique feature. Branching of lamellae during radial growth within a spherulitic superstructure occurs at the lateral {010} surfaces by homoepitaxial and tangential spherulitic growth.[13−17] The mesomorphic phase of quenched samples is characterized by a considerably smaller size of the crystalline domains into nanocrystals of about 100−200 Å if observed by electron microscopy and electron diffraction[12] or 30−50 Å if calculated from the line broadening of the wide-angle X-ray scattering (WAXS).[10,11] The crystallinity of quenched specimens is on the order of 35−40%, and the originally grown, small and conformationally disordered crystals anneal and reorganize by helix reversals to larger crystals.[18,19] The equilibrium melting temperature of the α-polymorph of iPP is 460.7 K, the heat of fusion is 8.7 kJ mol^{-1}, and the glass transition of the amorphous iPP is at 270 K, broadenend to higher temperature on partial crystallization, while the heat of transition from the conformationally disordered mesophase to the α-polymorph is only −0.6 kJ mol^{-1}.[20,21] The mesophase is metastable at temperatures below about 340 K; at room temperature it should be called a glassy mesophase.[19]

Isotactic polypropylene shows, in addition to irreversible crystallization and melting, a small amount of thermodynamically truly reversible crystallization and melting. Reversible crystallization and melting on polymers was quantitatively investigated in the past mainly by temperature-resolved small-angle X-ray scattering (SAXS) on well-crystallized polyethylene (PE)[22−25] and

† Martin-Luther-University Halle-Wittenberg.
‡ The University of Tennessee and Oak Ridge National Laboratory.

10.1021/ma010260g CCC: $20.00
Published on Web 07/13/2001

by temperature-modulated differential scanning calorimetry (TMDSC) on poly(ethylene terephthalate) (PET),[26,27] poly(oxyethylene) (POE),[28] poly(ether ether ketone) (PEEK),[29] polycaprolactone (PCL),[29,30] poly(ethylene-*co*-1-octene),[31] poly(ethylene-*co*-1-hexene),[32] poly(tetrafluoroethylene) (PTFE),[33] poly(trimethylene terephthalate) (PTT),[34] different paraffins as model compounds,[35] and polyethylene.[36] A series of six reversible and irreversible contributions to an apparent heat capacity have been identified as reversible vibrational and conformational contributions to the heat capacity (1 and 2, respectively). The reversible crystallization and melting (3) are separated from the irreversible primary (4) and secondary (5) crystallization and melting and finally the various irreversible annealing and crystal perfection processes (6).[31] In the present paper the reversible crystallization and melting (3) are separated from the other possible components to the apparent heat capacity and addressed as local thermodynamic equilibria at the crystal surface since the kinetic requirements of primary crystal, secondary, and molecular nucleation prior the crystallization would need supercooling.[37] For poly(ethylene-*co*-1-octene) reversible crystallization and melting has been suggested on the basis of standard DSC and TMDSC to occur on crystal surfaces or in intercrystalline regions.[38] Recently, the SAXS experiments of the earlier studies on polyethylene[22−25] with rather large temperature amplitude have been repeated with smaller amplitude, to be comparable to the temperature profiles in TMDSC.[39] The simultaneously recorded wide-angle and small-angle X-ray scattering point to a reversible temperature-triggered modulation of the crystallinity by variation of the crystal thickness of the lamellae at relatively high temperatures. The reversible crystallinity change obtained by X-ray scattering is about twice of the crystallinity change recorded by TMDSC. The mismatch was interpreted by a lowered heat of reversible transition, compared to the heat of irreversible melting/crystallization. The authors, however, did not discuss that {001} and related surfaces may accumulate larger concentrations of conformational defects close to the melting point which would yield reversible effects of type (2) to the apparent heat capacity and may cause the reversible increase of the lamellar thickness.[36,40]

In general, one assumes that the degree of reversibility of crystallization and melting is controlled by the constitution of the macromolecule and by the crystal morphology. One major influence of the molecular architecture is the capability of selected polymers to perform sliding diffusion of the chains within the crystal as the dominant mechanism for crystal thickening.[41,42] Polyethylene and poly(ethylene oxide) (PEO) are considered to have a high capability to undergo such sliding diffusion, whereas in iPP, PET, and PCL sliding diffusion is limited, and in syndiotactic PP no sliding diffusion was observed. In addition to the effect of the chemical structure, we have proven that the crystal morphology has a major effect on the degree of reversibility of crystallization and melting. It was qualitatively shown for a POE that the degree of reversibility of crystallization and melting increases if crystals are formed which are in a nonequilibrium condition, by variation either of the molar mass or of the crystallization conditions.[28] A quantitative relation between the degree of reversibility of crystallization and melting, the crystallization conditions, and the resulting crystal morphology has been established for poly(ethylene-*co*-1-octene) and revealed an increased degree of reversibility by about 10% if the cooling rate during main crystallization was increased by 1 order of magnitude.[31] The absolute value of reversible melting after cooling at 10 K min^{-1} from the not nucleated melt was about 0.1% K^{-1} at 298 K.[31] With increasing cooling rate, we have seen more and smaller, less perfect crystals which, together with the observation of an unchanged enthalpy-based crystallinity, explain the degree of reversibility of crystallization and melting to be controlled by the surface-to-volume ratio of the crystals without an unambiguous identification of the active surface.[31]

We selected in the presented study iPP to further probe the influence of the crystal morphology on the degree of reversibility of crystallization and melting under the condition of reduced sliding diffusion. Crystals of a different surface-to-volume ratio are created by variation of the crystallization conditions without significantly different overall crystallinity at elevated temperature, and we expect, thus, an effect on the degree of reversibility of crystallization and melting (effect 3). We consider this study as a continuation of our previous work to gain more insight into the mechanisms of the reversible crystallization and melting.

2. Experimental Section

2.1. Material. The material used in this study is a commercially available iPP of type KF 6190 H with an isotacticity index of 95−96% (Montell Polyolefins). The mass-average molar mass and the polydispersity are 373 kg mol^{-1} and 6.2, respectively, and the melt flow rate is 3.3 g (10 min)$^{-1}$ (503 K, 2.16 kg).[43] Thin films of thickness of about 200−300 μm were prepared in a Perkin-Elmer hot press and subsequently quenched in a mixture of dry ice/ethanol or ice water. Samples of different thermal history were prepared using the initial, quenched films via melting and recrystallization within a calorimeter or an X-ray temperature chamber, as described below.

2.2. Instrumentation. Standard differential scanning calorimetry (DSC) and temperature-modulated DSC (TMDSC) were performed using a Mettler-Toledo DSC 820 with a ceramic sensor FRS 5, equipped with a liquid nitrogen accessory. The furnace was purged with dry nitrogen at a flow rate of 80 mL min^{-1}. The large pan of 40 μL with a center pin was used in combination with the lid of the 20 μL pan in order to have maximum heat transfer into the thin sample from the top as well as from the bottom. The rate of temperature change was 10 K min^{-1}, if not stated otherwise. Temperature was set by the onset temperatures of melting of indium and zinc, and the heat flow rate was initially calibrated using the heat of fusion of indium. The apparent, total heat capacity was calculated from the heat flow rate after baseline correction and after a final calibration using a sapphire standard. The calculation of the temperature dependence of the enthalpy-based crystallinity was done by stepwise integration of the experimental apparent heat capacity down to an actual, crystallinity-corrected thermodynamic heat capacity baseline and normalization with the temperature-dependent enthalpy of fusion.[44,45] The enthalpy of fusion and thermodynamic heat capacity data were taken from the ATHAS database.[46] The TMDSC was performed using a sawtooth modulation of the program temperature with a modulation period of 240 s and a modulation amplitude of 1.0 or 2.0 K. The underlying heating rate $\langle q \rangle$ was 1 K min^{-1} or zero. The latter apply to quasi-isothermal experiments. The apparent reversing heat capacity, $C_p^{\#,\mathrm{rev}}$, was calculated as[47−49]

$$C_{\mathrm{p}}^{\#,\mathrm{rev}} = \frac{A_\Phi}{\omega A_{\mathrm{TS}}} K(\omega) \qquad (1)$$

with A_Φ and A_{TS} representing the amplitudes of the first harmonic of the Fourier series of the heat flow rate and sample temperature, respectively, ω is the modulation frequency (=2π/period), and $K(\omega)$ is a frequency-dependent calibration function. The value of $K(\omega)$ was set to unity since the selected low frequency of $2\pi/240$ rad s^{-1} in the case of the used Mettler-Toledo DSC 820 does not require a frequency calibration.[50] The degree of reversibility of crystallization and melting, $\Delta h_f^{reversible}$ in % per kelvin, was estimated from quasi-isothermal TMDSC experiments after the reversing component of the total heat capacity had reached equilibrium:[51]

$$c_p^{excess} = c_p^{reversing,\infty} - c_p^{thermodynamic};$$

$$100 \times \frac{c_p^{excess}}{\Delta h_f^{100}} = \Delta h_f^{reversible} \quad (2)$$

where c_p^{excess} is the excess specific heat capacity, which is calculated as difference between the specific, apparent, reversing heat capacity in equilibrium, $c_p^{reversing,\infty}$, and the specific thermodynamic heat capacity, $c_p^{thermodynamic}$, and Δh_f^{100} is the enthalpy of fusion of a 100% crystalline sample and is used as a normalizing factor. Note that the reversing apparent heat capacity may also contain irreversible latent heat contributions which are best recognized by long-term quasi-isothermal TMDSC and analysis of the higher harmonics of the Fourier series.

Wide-angle X-ray scattering (WAXS) was performed using a diffractometer URD 63 (Seifert-FPM) equipped with a low-temperature chamber TTK (Paar KG) and position-sensitive detector (STOE) and using Cu Kα radiation with a wavelength of 1.5418 Å. The measurements were done in the reflection mode with the quenched film specimens adjusted in height by aluminum oxide powder to avoid displacement errors[52] and to guarantee optimum heat transfer conditions between heater and sample in temperature-resolved experiments. A final check of the scattering angle was done by simultaneous measurement of the 111-reflection of calcium fluoride as a standard. The applied heating rate in the temperature-controlled experiments was 1.0 K min^{-1}. The temperature scale was checked by the melting temperatures of azobenzene and phenacetin measured by identical heating rates.

Atomic force microscopic studies were done using a Nano-Scope IIIa of Digital Instruments, Inc., with a standard Si cantilever, operated in the medium-tapping mode, and applying identical force and tip for the registration of each image. We have monitored the amplitude and the phase of the oscillation of the cantilever. Smooth surfaces of the samples were prepared by melting between sapphire disks, which are standard equipment for optical microscopy with a Leitz hot-stage, and subsequent quenching in a mixture of dry ice and ethanol or cooling at a rate of 10 K min^{-1}. Images were taken at ambient temperature before and after annealing at 413 K for 30 min. The annealing temperature of 413 K was reached by heating at a rate of 10 K min^{-1}, which permits a correlation of the calorimetric data to the microscopic images. Alternatively, we prepared samples without cover during melting and subsequent cooling, which resulted in identical images.

3. Results and Initial Discussion

3.1. General Thermal Behavior and Crystallinity. Figure 1 shows the apparent specific heat capacity of a quenched sample as a function of temperature during first heating (thick line), cooling (dotted line), and reheating (thin line). The symbols represent the thermodynamic heat capacities of amorphous (□) and crystalline iPP (◇).[46] With the help of these amorphous and crystalline baselines one can make a first assessment of the possible latent heat contributions to the apparent heat capacity. Both heating runs indicate the beginning of the glass transition at about 270 K. In the first heating run, the quenched sample shows a small endothermic event at about 320 K, somewhat above the glass transition temperature.[19] This is contiguously followed by a broad, structured exotherm, centered at about 367 K. It involves the transition of the mesophase glass to the α-polymorph and additional cold crystallization. Next is the main melting transition, which is completed at about 435−440 K.

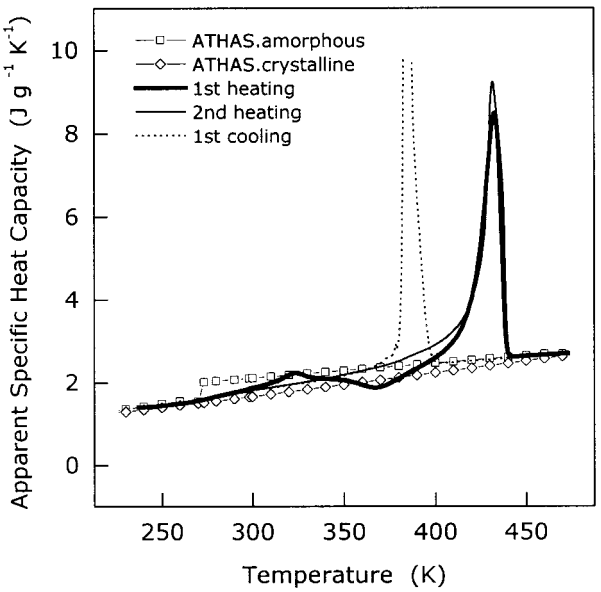

Figure 1. Apparent specific heat capacity of quenched iPP as a function of temperature during heating (first heating, solid thick line), cooling (dotted line), and reheating (second heating, solid thin line) at a rate of 10 K min^{-1}. The symbols are thermodynamic heat capacities of amorphous and crystalline iPP.

The cooling run at a rate of 10 K min^{-1} illustrates the large supercooling of about 40 K before crystallization, which is typical for polymers and makes the major portion of the crystallization and melting transition irreversible. The subsequent second heating scan reveals a very smooth glass transition, completed at about 300 K, followed by melting without detection of any discrete reorganization or recrystallization ranges. The temperature and enthalpy of the final melting peak above 400 K are almost independent of the thermal history, which shows that structural differences, evident at ambient temperature, are apparently largely removed or equalized during the heating of the samples.

Figure 2 shows the calculated changes of the enthalpy-based crystallinity as a function of temperature during heating of the quenched sample and the second heating run of the sample, which in the following discussion is referred to as the slowly cooled sample. The crystallinities are based on the apparent, specific heat capacities in Figure 1, calculated with the heat of fusion of the 100% crystalline α-polymorph. The enthalpy-based crystallinity of the quenched sample is about 36% at 298 K, compared to about 53% of the slowly cooled sample. The first endotherm of the quenched sample starts at about 310 K and is connected with a decrease of crystallinity by about 2−3%. Next, the quenched sample starts to reorganize to the α-polymorph at about 350 K with a heat of transition that can be estimated as being equivalent to about 2% ≈ 33% × 0.6 kJ mol^{-1}/8.7 kJ mol^{-1}. With the cold crystallization in the same temperature range, the sample reaches a maximum crystallinity of 40% at 390 K. The final melting begins at slightly higher temperature. The

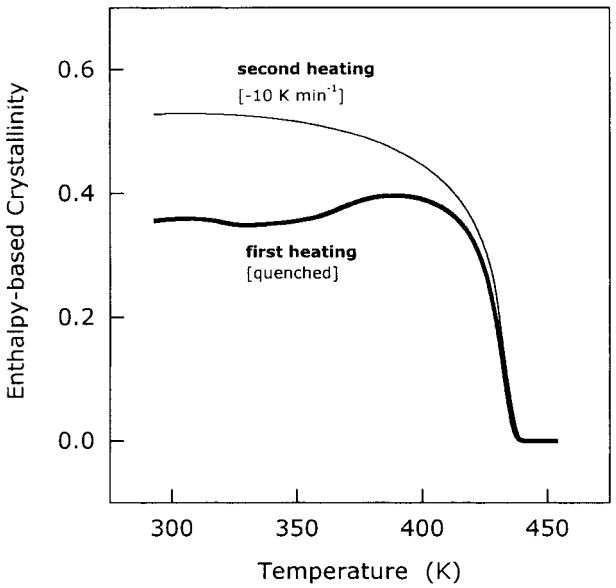

Figure 2. Enthalpy-based crystallinity of iPP as a function of temperature during heating. Samples were prepared by quenching in a mixture of dry ice/ethanol (lower curve, thick line) and by crystallization from the melt at a rate of 10 K min^{-1} (upper curve, thin line). The calculation was performed using the apparent specific heat capacity of the first and second heating scans shown in Figure 1.

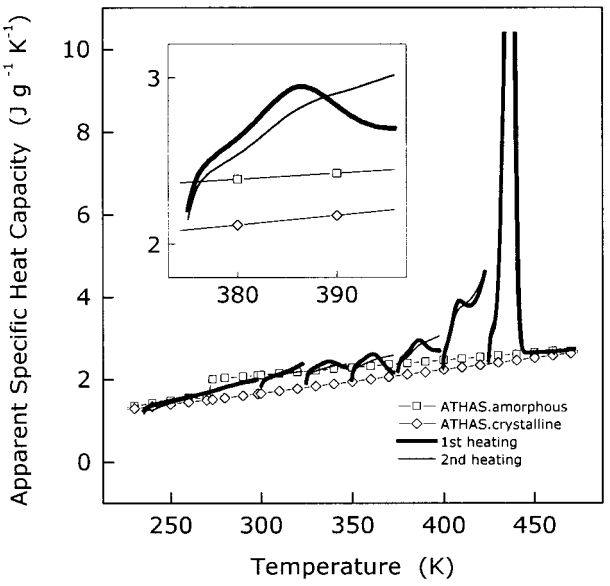

Figure 3. Apparent specific heat capacity as a function of temperature for a quenched sample (thick lines) and a sample which was cooled from the melt at a rate of 10 K min^{-1} (thin lines) during stepwise heating. The samples were isothermally annealed at 323 K for 40 min, at 348, 373, and 398 K for 100 min and at 423 K for 400 min. The inset shows the heating segment after annealing at 373 K.

slowly cooled sample shows a continuous, gradual decrease of crystallinity which starts at about 320 K. Its absolute value, however, remains always higher than the crystallinity of the quenched sample. Just before the final melting, the crystallinity difference between the quenched and slowly cooled sample becomes very small; it is only 3% at 423 K. One could assume that the structure and morphology of the crystalline phase and of the surrounding amorphous phase for the two samples apparently are very similar at this temperature since the subsequent melting shows practically no difference.

Needless to say, the measurement of the heat flow rate by standard DSC yields only integral values of exothermic and endothermic latent heats which are not resolvable. Furthermore, we have to admit that we rely on the crystallinity calculations on the heat of fusion of the perfect crystals of the α-polymorph, which is erroneous to some degree for the calculation of the enthalpy-based crystallinity of the quenched sample at low temperature, i.e., expressed in vol %, the changes in crystallinity may be even smaller than indicated.

The endotherm centered at 320 K on heating of the quenched sample above the glass transition of the amorphous fraction has the typical appearance of an annealing peak. This conclusion is verified by stepwise annealing experiments, illustrated in Figure 3. Both the quenched and slowly cooled samples were heated at a rate of 10 K min^{-1} to 323 K and annealed there for a period of 40 min, followed by further heating and annealing at 348, 373, and 398 K for periods of 100 min each and, at 423 K, for a period of 400 min. Figure 3 shows a small annealing peak about 10−15 K above each annealing temperature (see the example insert after annealing at 373 K). After each annealing peak, the apparent specific heat capacity decreases to the level of the unannealed sample as can be seen in Figure 1. The data show that the quenched sample has a much higher annealing tendency than the slowly cooled sample. The latter shows distinct annealing only at temperatures above 348 K. The estimated enthalpy change for the quenched sample is of the order of 1−5 J g^{-1}; i.e., each step increases the crystallinity by no more than 1−3%, which is reversed by the subsequent melting 10−15 K above the annealing temperature. Note that annealing at any particular temperature leads to arrested, metastable equilibria; i.e., subsequent increases of the temperature require new equilibration of the local structure. This can clearly be seen by the heating segment of the quenched sample from 348 to 373 K, which ends with a strong decrease of the apparent heat capacity into the minimum which was seen in Figure 1; i.e., the effect at about 370 K cannot be avoided by annealing at 20 K lower temperature. The reason for the occurrence of *arrested* metastable equilibria can be the requirement of prior melting of unstable crystals, which is temperature-dependent. Note that the annealing peaks are only linked to the cold crystallized or perfected crystals formed at the prior annealing temperature since there is no effect on the final melting peak.

The standard DSC was also used to study the heating rate dependence of the quenched sample. The low-temperature annealing-peak, the cold crystallization, and the final melting process were affected and gave information about the structure of the sample. The low-temperature melting peak shifts by about 15 K to higher temperature on increasing the heating rate from 1.0 to 100 K min^{-1}. It is most likely that the superheating of the imperfect crystals that give rise to the low-temperature endotherm is due to the surrounding amorphous phase which needs to be sufficiently mobile for quick fusion. The 320 K annealing peak may be too close to the glass transition for fast melting.[53] The cold crystallization at about 350 K is increasingly suppressed by higher heating rates. The crystallization may be hindered by the kinetics of crystallization, but also by the glass transition of the mesophase which precedes the transition to the α-polymorph. The suppression of the cold crystallization with increasing heating rate results

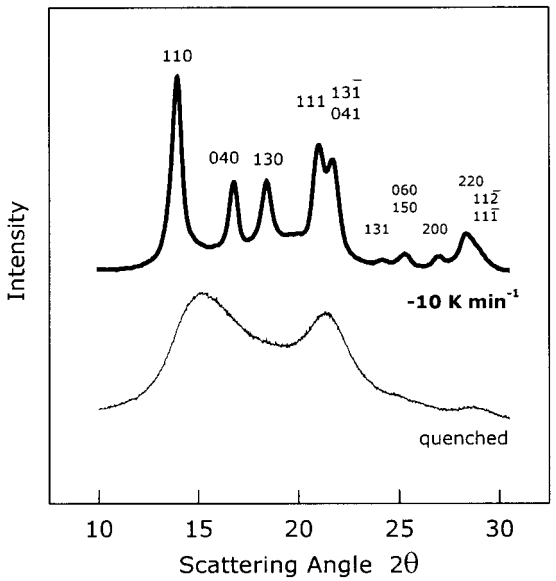

Figure 4. Plot of WAXS data of quenched and slowly cooled iPP. Peaks are marked by the Miller indices according to ref 4.

in a drop of the maximum crystallinity at 390 K by about 5%. The decreased maximum crystallinity can be used as a benchmark for poorer crystallization, but a *decrease* in the final melting peak position by about 5−10 K observed on faster heating suggests that all crystals improve during the slower heating, separate from the increased cold crystallization and reorganization of secondary crystals. These observations reveal clearly that on heating of a semicrystalline polymer one must separate the discussion of the major population of primary, high-melting crystals and the secondary, low-melting crystals. The reversibility of the transitions in both populations is most likely quite different.

3.2. X-ray Structure during Heating and Annealing. Figure 4 shows the wide-angle X-ray scattering diagram of the quenched and slowly cooled samples. The curves are vertically shifted for better comparison, and the diffraction peaks of the slowly cooled sample are indexed.[4] The scattering of the quenched sample is typical for the mesophase of iPP and shows beside the broad halos no separable crystalline reflections. The slowly cooled sample reveals the monoclinic α-polymorph as is expected for a non-*β*-nucleated material. Regardless of the absence of any obvious scattering of a crystalline phase in the case of the quenched sample, we have to keep in mind that its enthalpy-based crystallinity is 36% at 298 K, compared to 53% of the slowly cooled sample. Therefore, the absence of separable crystalline scattering in the case of the quenched sample must be due to extreme broadening of the diffraction lines, which need to be assigned to a very small crystal size and/or to a high concentration of paracrystalline defects which eliminate the internal symmetry of the crystalline domains.[54]

The annealing experiment by DSC in Figure 3 is repeated by X-ray diffraction in Figure 5a, using a similar temperature program. The quenched sample was heated in steps to the annealing temperatures of 373, 403, and 433 K followed by annealing for a period of 70 min at each step before the sample was finally melted. The data during the heating segments are drawn as thin lines, and the data during isothermal annealing are drawn as thick lines. Parts b and c of

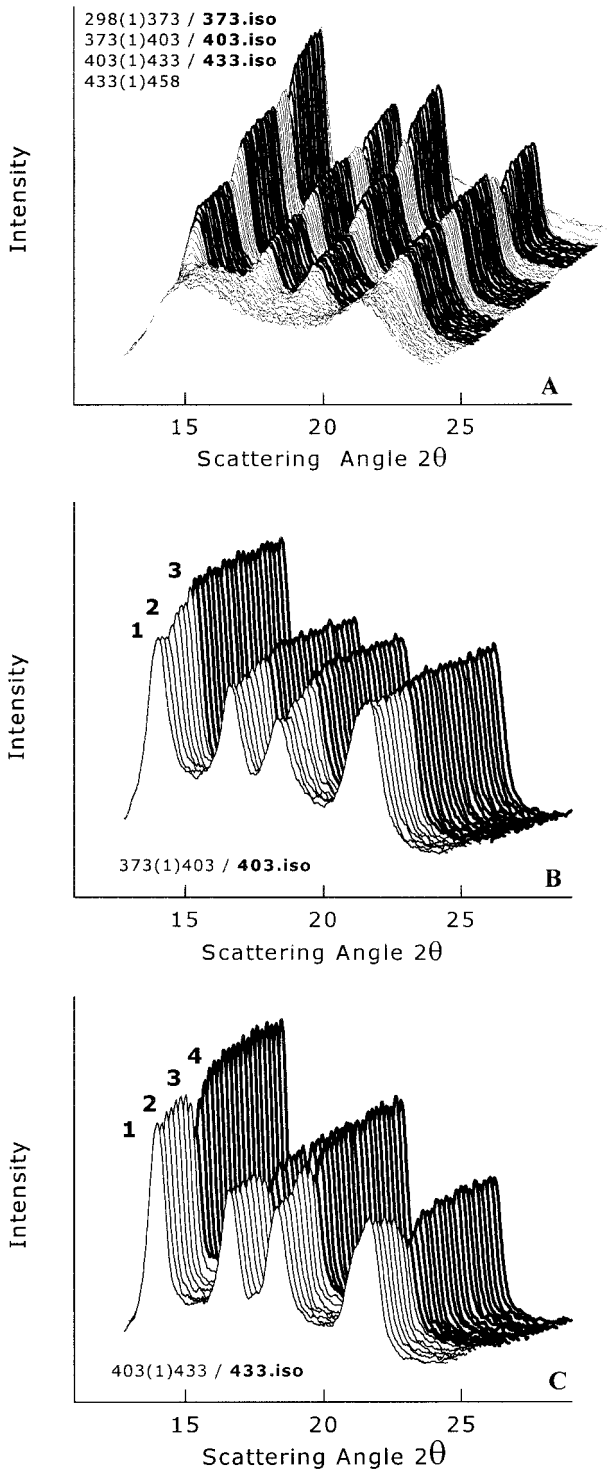

Figure 5. (a) Time-resolved WAXS of quenched iPP during continuous heating at a rate of 1 K min^{-1} with isothermal annealing steps. Annealing was performed at 373, 403, and 433 K for a period of 70 min. The thin-drawn lines represent data obtained during heating, and the thick-drawn lines represent data obtained during isothermal annealing. (b) Enlargement of (a), showing the heating segment from 373 to 403 K (thin lines) and the subsequent annealing segment at 403 K (thick lines). (c) Enlargement of (a), showing the heating segment from 403 to 433 K (thin lines) and the subsequent annealing segment at 433 K (thick lines).

Figure 5 are enlargements of the heating segments from 373 to 403 K and from 403 to 433 K, both with their subsequent annealing segments. The WAXS data in Figure 5a show that the mesophase of the quenched

sample starts to convert at about 350 K into the α-structure with typical long-range order, as one could calculate from the line broadening. At 373 K the isothermal annealing indicates within the first 5 min a very limited continuation of the conversion. No additional structural change is evident at the later times. Further heating from 373 to 403 K (Figure 5b) shows unchanged scattering for about 10 K (three scans, denoted as 1) before a further increase of the intensity of crystalline peaks reveals continued crystallization (2). The subsequent annealing at 403 K shows again only a very slight increase of the crystalline intensity in the beginning of the isothermal segment. The heating segment from 403 to 433 K (Figure 5c) shows again delayed continuation of the crystallization (1), continued crystallization (2), and, at about 423 K, beginning of melting (3). The melting process, however, gets disrupted by turning into the isothermal segment at 433 K, and the crystallinity increases again (4). Note that the apparent decrease of the intensity of the peak at 21.4 deg (2θ), on heating from 403 to 433 K, is not due to a decreasing crystallinity, but rather a further splitting of the 111 and 131/041 reflections. Finally, further heating converts the crystalline phase into the melt, as seen in Figure 5a.

The X-ray data can be explained in the context of the DSC discussion in the previous section. The beginning of the cold crystallization is detected by WAXS and by DSC at about 350 K, independent of the different heating rates of 1.0 and 10 K min^{-1}. The crystallization is strongly controlled by the actual temperature which only permits the equilibration of the structure into the arrested, metastable equilibrium. We have seen by DSC the very limited crystallinity increase on isothermal annealing by 3% or less, which coincides with the X-ray data, shown in particular in Figure 5b. The intensity of the crystalline peaks within the isothermal segment (thick lines) is almost unchanged and shows a minor increase just in the beginning of the annealing segment (see mark 3 in Figure 5b). Heating after annealing starts with a constant peak height (see mark 1 in Figure 5b,c), which goes along with the observed melting of the annealed crystals in the DSC analysis (the annealing peak in Figure 3). Further heating requires a new equilibration of the structure which in the case of the quenched sample is the continuation of secondary crystallization and crystal perfection (see mark 2 in Figure 5b,c). We are aware that the judgment of the recrystallization based on the peak maxima in the WAXS data is qualitative. It is clear that we cannot distinguish in this way between line-broadening effects and integral intensity effects. We know that it would perhaps be possible to separate secondary recrystallization and reorganization but consider such an accurate peak profile analysis as a separate study.

3.3. Morphology by AFM. Figure 6 shows AFM micrographs of the slowly cooled sample before (a) and after annealing (b) and of the quenched sample before (c) and after annealing (d). Annealing was performed at 413 K for a period of 30 min. The slowly cooled sample (10 K min^{-1}) (Figure 6a,b) exhibits a typical cross-hatched morphology of well-grown lamellae. The thickness of the lamellae before annealing is about 150−175 Å, and the lateral size in one direction is more than 1000 Å. The estimated long period L is about 200−300 Å and agrees reasonably well with the long period of 153 Å, which was obtained within a separate SAXS study using synchrotron radiation.[55] The lamellae thicken considerably during annealing to about 200−300 Å, which is consistent with earlier reports.[13] The quenched sample (Figure 6c,d) shows no organized crystalline−amorphous superstructure; i.e., neither lamellae nor distinct particle-shaped crystals are observed. The structure can at best be described to consist of regions of different structural order, perhaps of very small particles within a matrix of mesomorphic and/or amorphous structure. The small-angle X-ray scattering of the quenched sample revealed a Bragg distance of 81 Å, which points to the smallness of the crystalline domains but cannot unequivocally support the AFM micrograph. In Figure 6d we can see that, during heating of the quenched sample to 413 K and subsequent annealing for 30 min, particle-like crystals develop with a size of about 200−300 Å.

The morphology of the particular polypropylene which is used in this study and the results of the different thermal treatments and crystallization conditions are in good agreement with earlier studies. The crystalline domains in quenched iPP at ambient temperature exhibit a smectic symmetry with a size of about 75−100 Å[56] or a monoclinic symmetry with a size of about 100−200 Å.[12] The latter study gave also evidence of the existence of regions of "low level of crystalline order", which strongly supports our findings. Annealing at temperatures below the α-relaxation process, i.e., below about 393 K, does not change the domain size significantly, in contrast to annealing at temperatures above 393 K. After annealing at 411 K, the microcrystalline morphology is maintained, and the size of the nodules was reported to be increased to about 200−300 Å, with a tendency for lateral aggregation and merging of these crystalline particles.[56]

3.4. Degree of Reversibility of Crystallization and Melting. The degree of reversibility of crystallization and melting has been quantitatively measured by TMDSC. Figure 7 shows the reversing, apparent specific heat capacity of the quenched and slowly cooled samples as a function of temperature during continuous heating at an underlying heating rate $\langle q \rangle$ of 1.0 K min^{-1}. The reversing apparent specific heat capacity was calculated from the temperature-modulated heat flow rate according to eq 1 with $K(\omega) = 1$. The applied modulation amplitude and modulation period were 2.0 K and 240 s, respectively. The reversing apparent specific heat capacity of the quenched sample starts to get larger than that of the slowly cooled sample at about ambient temperature, just above the glass transition. The difference between the reversing apparent specific heat capacity of the quenched and slowly cooled samples gradually increases up to a temperature of ≈350 K, where the transition to the α-polymorph begins and remains then close to constant until final melting occurs. Even in the beginning of the melting range the reversing apparent specific heat capacity of the quenched sample remains larger than that of the slowly cooled sample.

The data of Figure 7, however, are of only limited use since information about true reversibility of a thermally activated process cannot be extracted quantitatively from them because of distortions arising from the possible presence of slow annealing, instrument lags, and phase transitions which may change with temperature and time.[57,58] Nevertheless, qualitatively one can judge the temperature dependence of partially reversing processes as filtered by the first harmonic of the Fourier series of the raw heat flow rate and the sample tem-

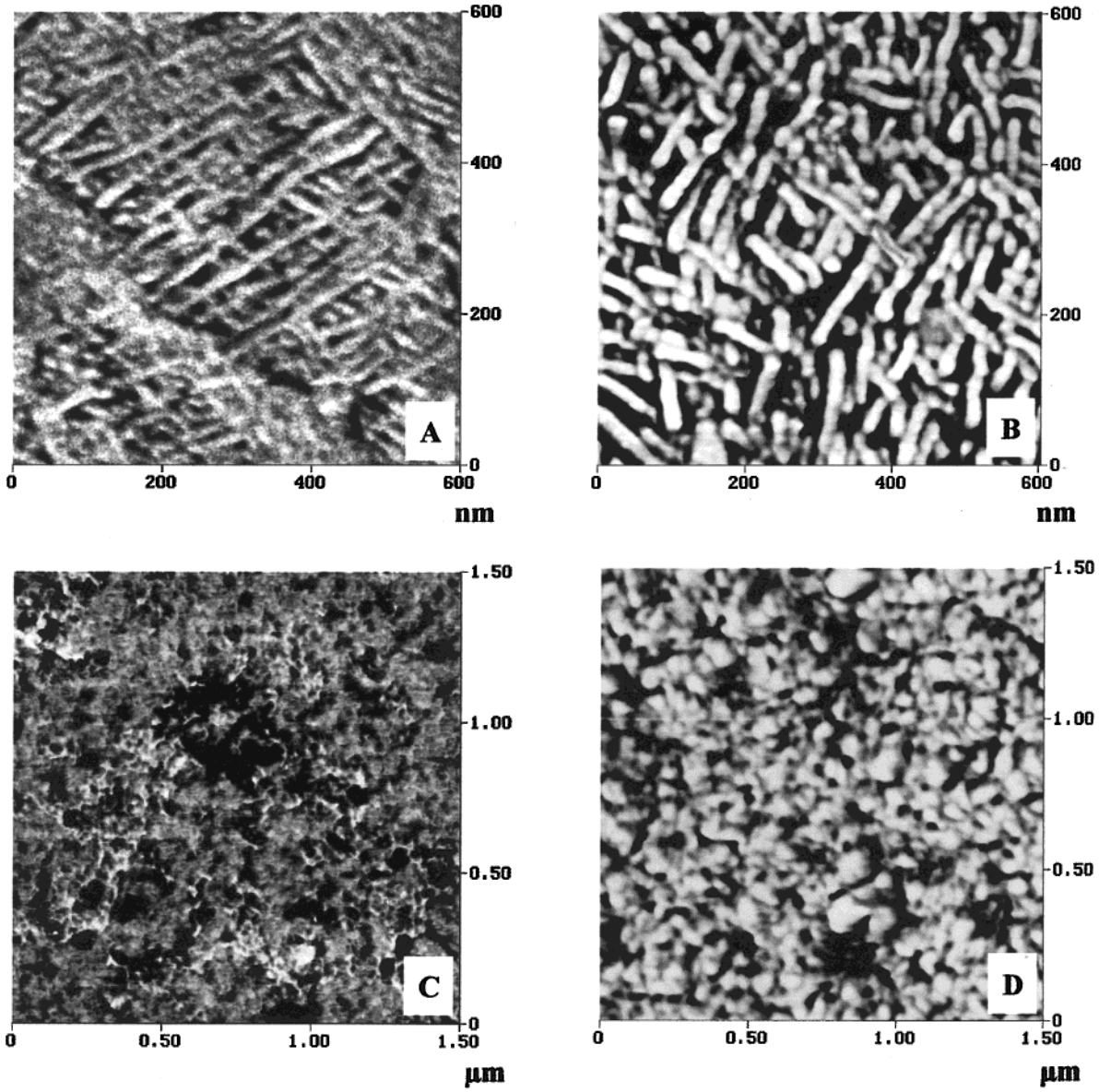

Figure 6. AFM micrographs of slowly cooled iPP before (a) and after annealing (b) and of quenched iPP before (c) and after (d) annealing. Annealing was performed at 413 K for a period of 30 min.

perature, as was proposed in the original patent of TMDSC.[59] Below a temperature of about 320 K the slowly cooled sample has an apparent reversing specific heat capacity which is only slightly larger than the thermodynamic heat capacity. The increase beyond the values of the completely crystalline polymer (◇) are due to the glass transition of the amorphous fraction, broadened, as usual, due to the partial crystallinity to about 290 K. No or only negligible irreversible and reversible latent heat exchanges occur up to 320 K in the case of the slowly cooled sample; i.e., the reversing apparent specific heat capacity is at the lowest possible value up to 320 K. At higher temperatures the reversing apparent specific heat capacity increases noticeably, which may be due to irreversible crystallization/melting within the time scale of the temperature modulation in addition to possible reversible processes. The quenched sample, in contrast, reveals an increased irreversible and/or reversible crystallization/melting starting right at the end of the glass transition temperature (≈300 K).

More accurate and detailed information can be gained by the separation of thermodynamically reversible and irreversible latent heat exchanges using quasi-isothermal TMDSC. Quasi-isothermal TMDSC extended over some sufficiently long time permits the irreversible processes to equilibrate and then shows the truly reversible latent heat effect. In Figure 8a the latent heat contribution to the reversible specific heat capacities of the quenched sample (□) and of the slowly cooled sample (■) are plotted as a function of temperature, as obtained by quasi-isothermal TMDSC after equilibrium has been reached. The data are normalized by subtraction of the thermodynamic heat capacity calculated from the values of the data bank and adjusted to the proper crystallinity. For comparison, we have added the data of Figure 7, which were obtained by TMDSC with $\langle q \rangle = 1.0$ K min^{-1}. The thick line represents data from the quenched sample, and the thin line, data from the slowly cooled sample. The arrows in Figure 8a show the decrease of the apparent specific heat capacity in both samples due to the irreversible processes, such as annealing and the

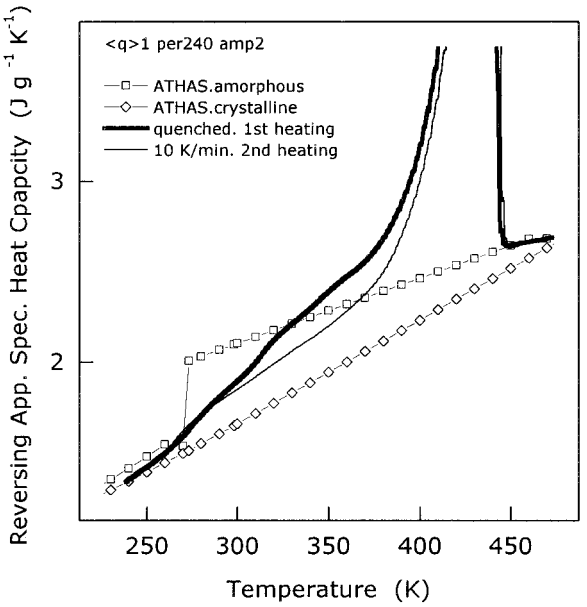

Figure 7. Reversing apparent specific heat capacity of quenched iPP (first heating) and of slowly cooled iPP (second heating) as a function of temperature on continuous heating at a rate $\langle q \rangle$ of 1 K min^{-1}. Heat capacities were calculated from TMDSC heat flow rate data according to eq 1, with $K(\omega) = 1$. The modulation amplitude and period were 2 K and 240 s, respectively. The symbols are thermodynamic heat capacities of amorphous and crystalline iPP, as given in the legend.

irreversible transition to the α-polymorph. We can see that the degree of the reversibility of the latent heat exchange decreases in both samples, leading to almost parallel curves beyond 320 K. The major increase in reversible effects starts for both samples at about 350 K. The increase in irreversible as well as reversible latent heat of the quenched sample beyond that of the slowly cooled sample develops between 300 and 320 K.

A direct comparison of the different degrees of reversibility of crystallization and melting between these two samples of different thermal history is given in Figure 8b. It presents a plot of the reversing apparent specific heat capacity of the quenched sample after subtraction of the thermodynamic specific heat capacity *and* the reversing apparent specific heat capacity of the slowly cooled sample (□). The degree of reversibility of crystallization and melting of the quenched sample increases immediately on heating above ambient temperature and reaches a constant offset at 350 K, the temperature of the beginning of the cold crystallization process obtained by standard DSC (see Figure 1). At approximately 380 K we see a further increase in the difference of reversible latent heats which leads to the final melting event.

The nonequilibrium data in Figure 8b, given by the thick line, clearly reveals the irreversibility of the cold crystallizations and the phase transition to the α-polymorph. The dotted line separates the three events as additional to the otherwise approximately constant difference. Note that the apparent reversing heat capacity registers both irreversible endotherms as well as exotherms which are not constant or changing linearly as positive, since it makes use of the always positive amplitudes of the first harmonic of the Fourier series (see eq 1, loss of stationarity[57,58]). One must, thus, compare the data with Figures 1 and 7 for full interpretation. The broad maximum can be linked to the first endotherm, followed by the exotherm, while the remaining additional rise between 340 and 370 K corresponds approximately to the change from the mesophase to α-polymorph transition. In addition to these three effects above the dotted line, the apparent, reversing specific heat capacity of the quenched sample decreases further by about 0.1 J g^{-1} K^{-1} before becoming fully reversible at a level substantially above that of the slowly cooled sample. This further improvement may be connected to the perfection of all crystals. The remaining difference, indicated by the shaded area, is the final difference in reversible melting between the

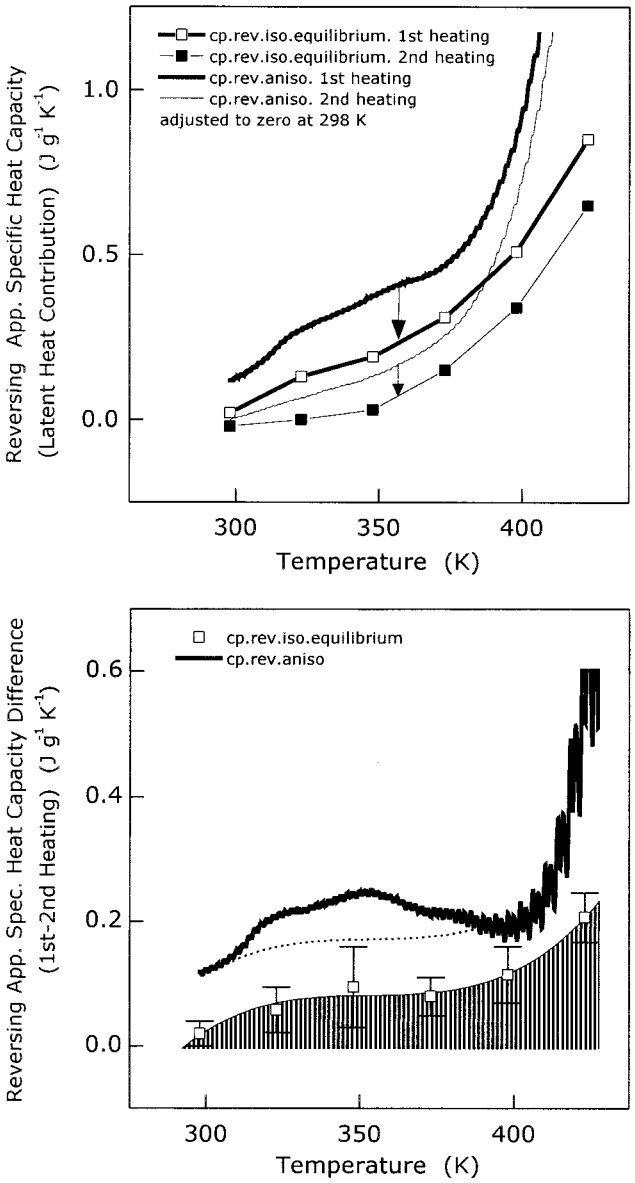

Figure 8. (a) Reversing apparent specific heat capacity after subtraction of the thermodynamic specific heat capacity for quenched and slowly cooled iPP as a function of temperature (open and filled symbols, respectively). Data by quasi-isothermal TMDSC after equilibrium has been reached. The thick and thin lines are reversing apparent specific heat capacities by TMDSC on quenched and slowly cooled iPP, respectively ($\langle q \rangle$ = 1 K min^{-1} as shown uncorrected for the thermodynamic heat capacity contribution in Figure 7). (b) Reversing apparent specific heat capacity of quenched iPP as a function of temperature, after subtraction of the thermodynamic specific heat capacity *and* the reversing apparent specific heat capacity of the slowly cooled sample. The open symbols represent data after equilibrium has been reached, and the thick line shows the TMDSC with $\langle q \rangle$ = 1 K min^{-1}.

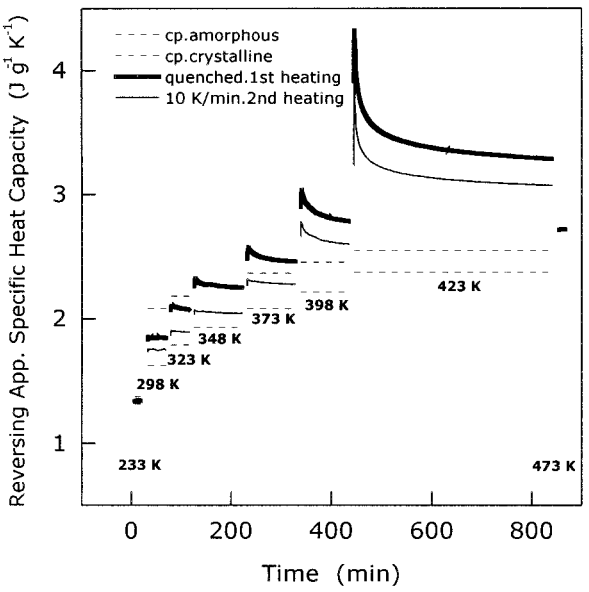

Figure 9. Reversing apparent specific heat capacity of quenched iPP (thick line) and slowly cooled iPP (thin line) as functions of time, during subsequent annealing at 298, 323, 348, 373, 398, and 423 K. The dotted lines are the thermodynamic specific heat capacity of amorphous and crystalline iPP.

quenched and slowly cooled sample. It becomes measurable above the glass transition, stays constant up to about 375 K all throughout the mesophase to α-polymorph transition and cold crystallization, and increases thereafter as major melting begins.

The detailed kinetics of the equilibration is shown in Figure 9. The reversing apparent specific heat capacities of the quenched (thick lines) and slowly cooled (thin lines) samples are plotted in the time domain for a series of temperatures. Additionally, we have added the thermodynamic heat capacity of the liquid amorphous and the crystal phase to show the distinct offset of the measured reversing and reversible apparent specific heat capacities. The data at 233 K, below the glass transition temperature, and at 473 K, above the melting temperature, were taken as internal calibration. The heating rate between the quasi-isothermal annealing segments was 10 K min^{-1}. The importance of the data, which are shown in Figure 9, is the (at least) two-step decay of the nonequilibrium, reversing specific heat capacity as a function of time. Without overinterpretation, one can conclude that there is a fast event in the beginning of every quasi-isothermal run during which annealing can take place. This fast process is followed by much slower equilibration. Such a separation is especially obvious at 348 K, the temperature where a major portion of the phase transition to the α-polymorph can take place at constant temperature.

4. Final Discussion and Conclusions

The scope of the presented study was to address the origin of the reversible crystallization and melting processes in isotactic PP. We have shown a distinct dependence of the degree of reversible crystallization and melting on the crystallization conditions and on the morphology of the crystalline phase as in a previous investigation on low crystalline poly(ethylene-*co*-1-octene).[31] Samples of iPP crystallized from the melt at higher cooling rates have an increased degree of reversibility of crystallization and melting over the entire temperature range between the glass transition and melting temperatures (see Figures 7−9). The quenched samples exhibit a reversible latent heat exchange of about 0.85 J g^{-1} K^{-1} at 423 K, compared to the slowly cooled sample with a reversible latent heat exchange of about 0.65 J g^{-1} K^{-1} (Figure 8a). The difference of 0.2 J g^{-1} K^{-1} at 423 K cannot be caused by a discrepancy in crystallinity of the quenched sample (see Figure 2). In standard DSC (Figures 1 and 3) and in TMDSC (Figure 7) one sees in this temperature range close to identical melting on heating of samples of different thermal history, and even the final heat of fusion is not largely different. The ultimate melting behavior, furthermore, depends not on the annealing history since isothermal annealing at lower temperature results in arrested equilibria (Figures 3 and 5). If one uses the final melting behavior as benchmark to judge the crystallinity and the internal structure of the crystals, one could easily make the mistaken conclusion that at 423 K totally identical structures are evident as the result of the recrystallization and reorganization processes of the quenched sample with an equilibration toward the structure of a slowly cooled sample.

The temperature of melting, T_m, is usually related to the heat of fusion of the perfect crystal, Δh_f^{100}, the fold-surface free energy, σ_e, the thickness of the lamellae, l_c, and the equilibrium melting temperature, T_m^o, as given by the Thomson−Gibbs equation:[53] $T_m = T_m^o[1 - 2\sigma_e/(l_c \times \Delta h_f^{100})]$. Only the equilibrium melting temperature, T_m^o, should be the same for both samples. The thickness of the lamellae l_c and the fold surface free energy can vary with crystallization condition and affect the experimentally observed melting temperature. Since in our case the melting temperatures are identical within 1 K, we have no arguments to assume sufficient differences between the samples with respect to σ_e and l_c. In addition, we have measured identical Bragg maxima at 423 K by SAXS which would give an equal thickness of lamellae with an assumed identical linear crystallinity.[55] Nonetheless, we need to be aware that the Thomson−Gibbs equation is always a simplification of the true situation since it neglects in the above form any further melting point depression by lateral surface free energies. The heat of fusion of the crystal Δh_f^{100} is also difficult to discuss since metastable crystals may have lower heats of fusion than the perfect crystal due to internal defects, as was derived, for example, for poly(ethylene-*co*-1-octene) by comparison of the enthalpic with the X-ray crystallinity.[60] Summarizing, we cannot conclude any structural difference from the melting behavior of the quench-crystallized and slowly crystallized samples using the Thomson−Gibbs equation and cannot explain the large difference of the degree of reversibility of crystallization and melting. Therefore, we will discuss the observed difference of the degree of reversibility of crystallization and melting using the AFM micrographs of Figure 6. At 423 K we see in the case of the quenched and annealed sample a globular structure of the crystalline domains, whereas in the case of the slowly cooled sample, even before annealing, we have well-grown and laterally extended lamellae. The WAXS gives an almost identical pattern at a temperature just below the melting point (see Figure 5a−c; further, more detailed WAXS studies are in progress), SAXS gives an identical invariant and Bragg maximum

at 423 K, and the standard DSC shows similar melting temperatures and heats of fusion at 10 K min^{-1} (although differences appear when comparing results at largely different heating rates; see section 3.1). The major difference between the samples is the degree of reversibility of crystallization and melting, which obviously is a very sensitive indicator of the crystalline morphology, as we proposed earlier.[31] In numerous investigations we have suggested, on the basis of quantitative analyses of the reversibility of the crystal/melt phase transition, that a relation to the crystal quality, order, and disorder exists. Without doubt the important parameter of the crystal quality is the total surface area and the local structure of the surface. In the present case, the lateral surface is the major variable, as shown in Figure 6 by the AFM micrographs. The globular crystals have similar fold-surface areas when compared to well-grown lamellae of low surface-to-volume ratio. Recent, but not yet published, data that were obtained on deformed ethylene copolymers point also to an increased specific lateral crystal surface which causes an increase of the reversible crystal−melt phase transition. [61]

Although the AFM patterns were taken at ambient temperature, after cooling from the annealing temperature at 10 K min^{-1}, we believe that the observed crystal morphology qualitatively is not affected by the additional cooling step; i.e., we assume absent irreversible crystallization during cooling which could cause a decoration of not-visible crystals and misinterpretation of the micrographs. Most of the crystallinity gain during cooling after annealing at elevated temperature is due to reversible crystallization, which, based on the data in Figures 7−9, can easily accumulate up to ≈20% in the case of the quenched sample, when using the heat of irreversible crystallization or melting for normalization, respectively. And a further, strong indication of absent nonreversing crystallization and melting during cooling from the annealing temperature down to ambient temperature is given by an absolutely unchanged reversibility of crystallization/melting after reheating to the annealing temperature.

The questions remain why are the melting temperatures equal with large differences in lateral surface areas and why does the side surface affect the fraction of reversible melting? If the specific surface area is increased, the crystal should melt at lower temperature, assuming that the surrounding melt is relaxed and the bulk heat of fusion unchanged. Our knowledge about surface free energies of polymer crystals requires, however, considerable strain at the surfaces that include chain ends, folds, or cilia. Typically, the side-surface energy is assumed to be smaller by a factor of about 1/10.[37,53] We may suggest, thus, that the lateral surface energy affects the melting temperature so much less that experimentally this has not been noticed. It has also been argued that internal lateral surfaces (grain boundaries, invoked to explain the smaller X-ray coherence lengths than the lamellar widths) may decrease the differences between globular crystals and lamellae of similar fold lengths.

The locally reversible melting or disordering must be coupled with crystallization or ordering processes free of nucleation. The effect (2) is not considered of as much importance in iPP as in polyethylene. The heat capacity of iPP seems fully vibrational up to the beginning of melting, although difficulties exist in the analysis at higher temperature due to a variable rigid amorphous fraction.[20] This leaves true phase transitions as main reasons for the reversible latent heat (effect 3). At low temperature short chain segments may be added and removed to crystals, and even new crystals may be formed as secondary crystals without need of nucleation, as was recently proven for paraffins[35] and applies also for polyethylene fractions of lengths up to about 75 chain atoms.[36] For longer segments, as must be involved in the main melting peak, reversibility requires the absence of molecular nucleation,[62] as proposed earlier.[26,28] We have discussed these reversible crystallization and melting phenomena also in poly(ethylene-*co*-1-octene).[31] With the knowledge that in this case the crystal thickness/height is fixed by the temperature-dependent selection process of the ethylene sequences on crystallization, reversible growth in the longitudinal chain direction is hindered. The present model does not require any large-distance diffusion of chain segments through the crystal which may be possible in homopolyethylene, but not in poly(ethylene-*co*-1-octene) and iPP. Rather, a reversible detachment and attachment of some chain segments can occur at the crystal surface. At low temperatures these chain segments are so short that nucleation is not necessary, while at high temperature there must be long segments which melted partially and leave molecular nuclei on the remaining crystal which permit reversibility. The time-dependent decrease in reversing, apparent heat capacity is mainly due to annealing during the recrystallization (effect 6).

Summarizing, the combination of quantitative standard DSC, TMDSC, X-ray diffraction, and AFM has permitted the study of several new processes that occur on heating of iPP and also exist in other semicrystalline polymers. In particular, we have measured a substantial increase of the degree of locally reversible crystallization and melting within the metastable, global structure in quenched, isotactic polypropylene when compared to slowly crystallized specimens. The crystallinity, the heat of fusion, the melting temperature, and structural data obtained by WAXS and SAXS are insensitive to these changes and give at the used level of precision no suggestion of how the increased reversibility of crystallization and melting can be explained. From AFM studies we conlude that the crystalline domains are different in shape. In particular, we can see a considerably larger lateral surface area, resulting from the globular structure of the crystals in the quenched sample and, thus, suggest that most of the reversible melting of iPP resides at these surfaces. Recrystallization and reorganization results in growth of the domains without change in the overall shape. It is easily linked to the decrease with time in the reversing heat flow rate until only the reversible melting and crystallization remains.

Acknowledgment. The authors gratefully acknowledge technical assistance in the AFM study by R. Adhikari from the group of Prof. G. Michler (Martin-Luther-University Halle-Wittenberg). Some of the work was supported by the Division of Materials Research, National Science Foundation, Polymers Program, Grant DMR-9703692, and the Division of Materials Sciences and Engineering, Office of Basic Energy Sciences, U.S. Department of Energy at Oak Ridge National Laboratory, managed and operated by UT-Batelle, LLC, for the U.S. Department of Energy, under Contract DOE-AC05-00OR22725.

References and Notes

(1) Natta, G.; Corradini, P. *Nuovo Cimento Suppl.* **1960**, *15*, 40.
(2) Keith, H. D.; Padden, F. J., Jr.; Walter, N. M.; Wyckoff, H. W. *J. Appl. Phys.* **1959**, *30*, 1485.
(3) Turner Jones, A.; Aizlewood, J. M.; Beckett, D. R. *Makromol. Chem.* **1964**, *75*, 134.
(4) Meille, S. V.; Ferro, D. R.; Brückner, S.; Lovinger, A. J.; Padden, F. J. *Macromolecules* **1994**, *27*, 2615.
(5) Addink, E. J.; Beintema, J. *Polymer* **1961**, *2*, 185.
(6) Meille, S. V.; Brückner, S.; Porzio, W. *Macromolecules* **1990**, *23*, 4114.
(7) Miller, R. L. *Polymer* **1960**, *1*, 135.
(8) Natta, G.; Peraldo, M.; Corradini, P. *Rend. Accad. Naz. Lincei* **1959**, *26*, 14.
(9) Guerra, G.; Petraccone, V.; de Rosa, C.; Corradini, P. *Makromol. Chem., Rapid Commun.* **1985**, *6*, 573. Corradini, P.; Petraccone, V.; de Rosa, C.; Guerra, G. *Macromolecules* **1986**, *19*, 2699. Corradini, P.; de Rosa, C.; Petraccone, V.; Guerra, G. *Polym. Commun.* **1989**, *30*, 281.
(10) Bodor, G.; Grell, M.; Kallo, A. *Faserforsch. Textiltechnik* **1964**, *15*, 527.
(11) McAllister, P. B.; Carter, T. J.; Hinde, R. M. *J. Polym. Sci., Polym. Phys.* **1978**, *16*, 49.
(12) Caldas, V.; Brown, G. R.; Nohr, R. S.; MacDonald, J. G.; Raboin, L. E. *Polymer* **1994**, *35*, 899.
(13) Norton, D. R.; Keller, A. *Polymer* **1985**, *26*, 704.
(14) Bassett, D. C.; Olley, R. H. *Polymer* **1984**, *25*, 935. Olley, R. H.; Bassett, D. C. *Polymer* **1989**, *30*, 399.
(15) Padden, F. J., Jr.; Keith, H. D. *J Appl. Phys.* **1966**, *37*, 4013.
(16) Lotz, B.; Wittmann, J. C. *J. Polym. Sci., Polym. Phys.* **1986**, *24*, 1541.
(17) Binsbergen, F. L.; de Lange, B. G. M. *Polymer* **1968**, *9*, 23.
(18) Fichera, A.; Zannetti, R. *Makromol. Chem.* **1975**, *176*, 1885. Zannetti, R.; Celotti, G.; Fichera, A.; Francesconi, R. *Makromol. Chem.* **1969**, *128*, 137.
(19) Wunderlich, B.; Möller, M.; Grebowicz, J.; Baur, H. Conformational Motion and Disorder in Low and High Molar Mass Crystals. *Adv. Polym. Sci.* **1988**, *87*, 57 ff.
(20) Grebowicz, J.; Lau, S.-F.; Wunderlich, B. *J. Polym. Sci., Polym. Symp.* **1984**, *71*, 19. Bu, H.-S.; Cheng, S. Z. D.; Wunderlich, B. *Makromol. Chem., Rapid Commun.* **1988**, *9*, 75.
(21) Wunderlich, B. *Macromolecular Physics*; Academic Press: New York, 1973; Vol. 1.
(22) Strobl, G. R.; Schneider, M. J.; Voigt-Martin, G. J. *J. Polym. Sci., Polym. Phys.* **1980**, *18*, 1361.
(23) Schultz, J. M.; Fischer, E. W.; Schaumburg, O.; Zachmann, H. A. *J. Polym. Sci., Polym. Phys.* **1980**, *18*, 239.
(24) Tanabe, Y.; Strobl, G. R.; Fischer, E. W. *Polymer* **1986**, *27*, 1147.
(25) Albrecht, T.; Strobl, G. *Macromolecules* **1995**, *28*, 5827.
(26) Okazaki, I.; Wunderlich, B. *Macromolecules* **1997**, *30*, 1758; *Macromol. Chem. Phys., Rapid Commun.* **1997**, *18*, 313.
(27) Schick, C.; Merzlyakov, M.; Wunderlich, B. *Polym. Bull.* **1998**, *40*, 297.
(28) Ishikiriyama, K.; Wunderlich, B. *Macromolecules* **1997**, *30*, 4126; *J. Polym. Sci., Polym. Phys.* **1997**, *35*, 1877.
(29) Wurm, A.; Merzlyakov, M.; Schick, C. *Colloid Polym. Sci.* **1998**, *276*, 289. Wurm, A.; Merzlyakov, M.; Schick, C. *J. Macromol. Sci., Phys.* **1999**, *B38*, 693.
(30) Wurm, A.; Merzlyakov, M.; Schick, C. *J. Therm. Anal.* **1999**, *56*, 1155.
(31) Androsch, R. *Polymer* **1999**, *40*, 2805. Androsch, R.; Wunderlich, B. M*acromolecules* **1999**, *32*, 7238; **2000**, *33*, 9076.
(32) Androsch, R., unpublished data.
(33) Androsch, R. *J. Polym. Sci., Polym. Phys.* **2001**, *34*, 750.
(34) Pyda, M.; Wunderlich, B. *J. Polym. Sci., Polym. Phys.* **2000**, *38*, 622.
(35) Pak, J.; Wunderlich, B. *J. Polym. Sci., Polym. Phys.* **2000**, *38*, 2810.
(36) Pak, J.; Wunderlich, B. *Macromolecules* **2001**, *34*, 4492.
(37) Wunderlich, B. *Macromolecular Physics*; Academic Press: New York, 1976; Vol. 2,
(38) Alizadeh, A.; Richardson, L.; Xu, J.; McCartney, S.; Marand, H.; Cheung, Y. W.; Chum, S. *Macromolecules* **1999**, *32*, 6221.
(39) Goderis, B.; Reynaers, H.; Scherrenberg, R.; Mathot, V. B. F.; Koch, M. H. J. *Macromolecules* **2001**, *34*, 1779.
(40) Sumpter, B. G.; Noid, D. W.; Liang, G. L.; Wunderlich, B. *Adv. Polym. Sci.* **1994**, *116*, 27.
(41) Hikosaka, M.; Seto, T. *Polym. J.* **1973**, *15*, 111. Blais, J.; Manley, R. *J. Macromol. Sci., Part B* **1967**, *1*, 525.
(42) Hu, W.; Albrecht, Th.; Strobl, G. *Macromolecules* **1999**, *32*, 7548.
(43) Private communication, Basell Bayreuth Chemie GmbH, 2001.
(44) Mathot, V. B. F. *Calorimetry and Thermal Analysis of Matter*; Hanser Publishers: München, 1994; p 105.
(45) Wunderlich, B. *Thermal Analysis*; Academic Press: Boston, 1990.
(46) *A*dvanced *TH*ermal *A*nalysis *S*ystem; Wunderlich, B. *Pure Appl. Chem.* **1995**, *67*, 1919. For downloadable data use WWW (Internet): URL: http://web.utk.edu/~athas.
(47) Wunderlich, B.; Jin, Y.; Boller, A. *Thermochim. Acta* **1994**, *238*, 277.
(48) Androsch, R.; Moon, I.; Kreitmeier, S.; Wunderlich, B. *Thermochim. Acta* **2000**, *357*−*358*, 267.
(49) Androsch, R.; Wunderlich, B. *Thermochim. Acta* **1999**, *333*, 27.
(50) Androsch, R. *J. Therm. Anal. Calorim.* **2000**, *61* (1), 75.
(51) Androsch, R.; Wunderlich, B. *Thermochim. Acta* **2001**, *369*, 67.
(52) Bish, D. L.; Post, J. E. *Reviews in Mineralogy*; The Mineralogical Society of America: Washington, DC, 1989; Vol. 20.
(53) Wunderlich, B. *Macromolecular Physics*; Academic Press: New York, 1980; Vol. 3.
(54) Alexander, L. E. *X-ray Diffraction Methods in Polymer Science*; Wiley-Interscience: New York, 1969.
(55) Androsch, R.; Goderis, B.; Reynaers, H.; Mathot, V. B. F.; Koch, M. H. J., unpublished data.
(56) Hsu, C. C.; Geil, P. H.; Miyaji, H.; Asai, K. *J. Polym. Sci., Polym. Phys.* **1986**, *24*, 2379.
(57) Wunderlich, B.; Boller, A.; Okazaki, I.; Ishikiriyama, K.; Chen, W.; Pyda, M.; Pak, J.; Moon, I.; Androsch, R. *Thermochim. Acta* **1999**, *330*, 21.
(58) Merzlyakov, M.; Schick, C. *Thermochim. Acta* **1999**, *330*, 55.
(59) Reading, M.; Hahn, B. K.; Crowe, B. S. U.S. Patent, Method and Apparatus for Modulated Differential Analysis, 5,224,-775, July 6, 1993. Gill, P. S.; Sauerbrunn, S. R.; Reading, M. *J. Therm. Anal.* **1993**, *40*, 931. Reading, M.; Luget, A.; Wilson, R. *Thermochim. Acta* **1994**, *138*, 295.
(60) Androsch, R.; Blackwell, J.; Chvalun, S. N.; Wunderlich, B. M*acromolecules* **1999**, *32*, 3735.
(61) Androsch, R.; Wunderlich, B., to be submitted for publication in M*acromolecules*.
(62) Wunderlich, B. *Discuss. Faraday Soc.* **1979**, *68*, 239.

MA010260G